Research Article

Influence of Samarium on Structural, Morphological, and Electrical Properties of Lithium Manganese Oxide

B. Narenthiran,[1] S. Manivannan ⓘ,[2] S. Sharmila,[3] A. Shanmugavani,[4] and Perumalla Janaki Ramulu ⓘ[5]

[1]*Department of Mechanical Engineering, Karpagam Academy of Higher Education, Coimbatore, India*
[2]*Centre for Material Science, Department of Mechanical Engineering, Karpagam Academy of Higher Education, Coimbatore, India*
[3]*Department of Physics, Karpagam Academy of Higher Education, Coimbatore, India*
[4]*Department of Physics, Sri GVG Visalakshi College for Women, Udumalpet, Tamil Nadu, India*
[5]*Department of Mechanical Engineering, Adama Science and Technology University, Adama, Ethiopia*

Correspondence should be addressed to Perumalla Janaki Ramulu; perumalla.janaki@astu.edu.et

Research and developments on preparing electrode material for lithium-ion batteries are burgeoning nowadays widely. In this study, we used the high energy ball-milling method to prepare pure and samarium-doped lithium manganese oxide ($Li_4Mn_5O_{12}$) and investigated its structural, morphological, and electrical properties. The XRD spectrum for the produced materials confirmed the phase purity and crystallinity of the material. The fourier transform infrared spectrum was used to determine the different sorts of vibrations between molecules. The particle size with the presence of polyhedral-shaped morphology was certified by using SEM and TEM analysis. EDS mapping was used to assess the elemental composition and purity of the samples. Complex impedance spectroscopy analysis was used to investigate the temperature dependency of the materials' electrical properties, and high conductivity (1.15×10^{-7} S cm^{-1}) was reported for samarium-doped lithium manganese oxide at 100°C, and its dielectric relaxation behavior was examined.

1. Introduction

It is proven that lithium-ion batteries (LIBs) are the most important candidates in electrochemical energy storage systems. In the past decade, rechargeable Li-ion batteries were widely used in portable electronics and in electric vehicles (EVs) due to their high energy density [1, 2]. However, the lack of specific capacity and power density is a major difficulty in meeting the current energy requirements. Some of the materials such as $LiCoO_2$ [3, 4], $LiFePO_4$ [5, 6], $LiMn_2O_4$ [7–9], and $LiMn_xNi_yCo_zO_2$ [10–13] are investigated widely as cathode materials. Among them, $Li_4Mn_5O_{12}$ is a promising cathode material yet to be commercialized for novel cathode material with high energy density, low cost, and better safety. Thus, it is very important to explore its physicochemical properties through structural, morphological, and electrical properties.

Lithium manganese oxide spinels (LMO) are technologically important cathode materials with Mn in the +3 or +4 oxidation state. It also exhibits good electrical conductivity (10^{-6} S cm^{-1}), good rate capacity, high electrode potential, low cost, and is easily available and safer. However, this material encounters severe capacity fading upon cycling. This is because it crystallizes as spinels, the rock salt structure Li_2MnO_3, or as orthorhombic $LiMnO_2$ with a corrugated structure (o-$LiMnO_2$). In the spinel phase, the Mn^{4+}/Mn^{3+} reaction leads to severe Mn dissolution and Jahn Teller distortion, and the average valence of Mn falls below +3.5.

As a result, the structural integrity of the unit cell is collapsed during repeated charging/discharging and it thus losses its cycling performance.

However, the oxidation state of +4 in the $Li_4Mn_5O_{12}$ makes it an impressive cathode material with its theoretical capacity of 163 mAhg^{-1} for researchers. The recent works with the improved electrochemical performance of lithium excess layered cathode (LLC) $Li_4Mn_5O_{12}$ with spinel/layered heterostructure have been reported [14, 15]. Also, the $Li_4Mn_5O_{12}$ spinel phase has less lattice mismatch with the host layered structure and is favorable for the Li + ion diffusion. Also, the higher oxidation of Mn + 4 suppresses Jahn–Teller distortion and this results in a better cycling performance than $LiMn_2O_4$.

Furthermore, synthesizing pure $Li_4Mn_5O_{12}$ is a challenging task since at 400°C or above, the tetra valence manganese ions reduce to trivalent manganese ions and form $LiMn_2O_4$ and Li_2MnO_3. Hence, it requires multistep methods to produce $Li_4Mn_5O_{12}$. In common, the solid-state method is employed to prepare these materials. However, the solid-state method does not produce any specified morphology and also exhibits a larger particle size. It is well known that the aforementioned parameter has a significant effect on the electrical and electrochemical performance. Hence, for the present work, a high-energyball-milling method is employed to synthesize the $Li_4Mn_5O_{12}$ particles.

In this line, to increase the electrochemical performance of $Li_4Mn_5O_{12}$, one of the important strategies is the doping of rare earth elements. Ram Pura et al. have doped the various rare earth elements such as neodymium (Nd) and gadolinium (Gd) into the $LiMn_2O_4$ to increase the electrochemical performance [16]. Similarly, heavy rare earth (Er, Sc, Y, etc.)-doped $LiMn_2O_4$ has been reported in the literature [17]. Despite of its expensiveness, rare earth material has drawn more attention recently. Furthermore, the reported works of $LiMn_{2-x}RE_xO_4$ (RE = La, Ce, Nd, and Sm; $0 \le x \le 0.1$) have provided information regarding the influence of doping light rare earth elements on the $LiMn_2O_4$ and its electrochemical performance [18].

Many research studies reported the electrochemical performance of the $Li_4Mn_5O_{12}$ since it is a material used for the cathode in the Li-ion battery. Scarcely, reports had reported the electrical performance of these LMO materials. Sharmila et al. [19–23] have reported the conductivity of optimized Co-doped $Li_4Mn_{4.5}Co_{0.5}O_{12}$ (3.1×10^{-5} S cm^{-1}) and Ni-doped $Li_4Mn_{4.9}Ni_{0.1}O_{12}$ (7.01×10^{-5} S.cm^{-1}) at 433 K and 393 K, respectively. Similarly, for Mo-doped ($Li_2Mn_{3.75}Mo_{0.25}O_9$) and Ti-doped $Li_4Mn_{4.7}Ti_{0.3}O_{12}$, the maximum conductivity is reported as 7.44×10^{-6} S cm^{-1} and 1×10^{-5} S cm^{-1} at 413 and 393 K, respectively. The effect of Zr doping on the conductivity was reported for the molten synthesized $Li_4Mn_{4.9}Zr_{0.1}O_{12}$ at 160°C as 1.4×10^{-5} S cm^{-1}. However, the effect of Sm doping on the $Li_4Mn_5O_{12}$ is scarcely reported. In this line, the present work attempts to study the influence of samarium on the structural, morphological, and electrical performance of the prepared $Li_4Mn_5O_{12}$ particle.

2. Experimental Methods

A combination of the solid-state method and ball-milling method has been employed to prepare pure and samarium-doped lithium manganese oxide ($Li_4Mn_5O_{12}$). Lithium hydroxide monohydrate (LiOH.H$_2$O), manganese dioxide (MnO$_2$), and ethanol purchased from SRL, Mumbai, India, are used as a raw materials without any further modifications; samarium (III) oxide (Sm$_2$O$_3$) is used as a raw material for metal dopant. A stoichiometric amount of LiOH.H$_2$O and MnO$_2$ was ground individually in a mortar and pestle for 30 minutes and then mixed together. The mixer was then transferred to a Fritsch Pulversiette 7 Planetary Ball Mill consisting of zirconia balls. Ethanol is used as a solvent to reduce friction and heat generated during milling which may also help avoid damage occuring on the surface of the balls. The mixer is milled for a period of 8 h with 10 minutes rest for each and 30 minutes grinding. The sample-to-ball mass ratio is fixed as 1 : 3 with a rotation speed of 300 rpm, and after complete grinding, the sample is calcined at 800°C for 10 h. The obtained powder is ground and utilized further for characterization. Samarium-doped lithium manganese oxide-$Li_4Mn_{4.75}Sm_{0.25}O_{12}$was prepared uisng the aforementioned procedure and conditions. The final compounds are named as LM (pure) and LS (samarium dope) for further discussion.

2.1. Material Characterization.
The XRD spectrum is recorded for the prepared samples to identify the structure and phase purity by using (BRUKER) Cu-Kα radiations with 2θ in the range of 10° to 80° with a scan speed of 10°/min. The presence of functional groups is analyzed by using the fourier transform infrared spectrophotometer. The morphology, shape, and size of the prepared cathode materials are investigated by the scanning electron microscope (TESCAN, VEGA3 SBH) and transmission electron microscope (Tecnai G2 20 S-TWIN) along with elemental analysis by EDX spectrum and mapping. The lattice fringes and planes are studied with the help of the SAED pattern. A computer-controlled HIOKI 3532 LCR HI-TESTER was used to measure the impedance and conductivity of both the samples throughout a range of temperatures, from 40 to 100°C and 100 KHz to 5 MHz.

3. Results and Discussion

Figure 1 represents the XRD analysis of the pristine ($Li_4Mn_5O_{12}$-LM) and samarium-doped lithium manganese oxide ($Li_4Mn_{4.75}Sm_{0.25}O_{12}$-LS). The spectrum indicates the formation of highly crystalline, sharp, and well-defined peaks matched with earlier reports and JCPDS card No. 46-0810 [19–21]. The diffraction peaks of LM attribute to (111), (311), (400), (331), (511), (440), and (531) planes and correspond to d-spacing: 4.732, 2.467, 2.045, 1.861, 1.575, 1.556, and 1.385 Å, respectively. All the characteristic peaks attribute to a cubic spinel structure with the *fd3m* space group. No changes have been observed in its structure by
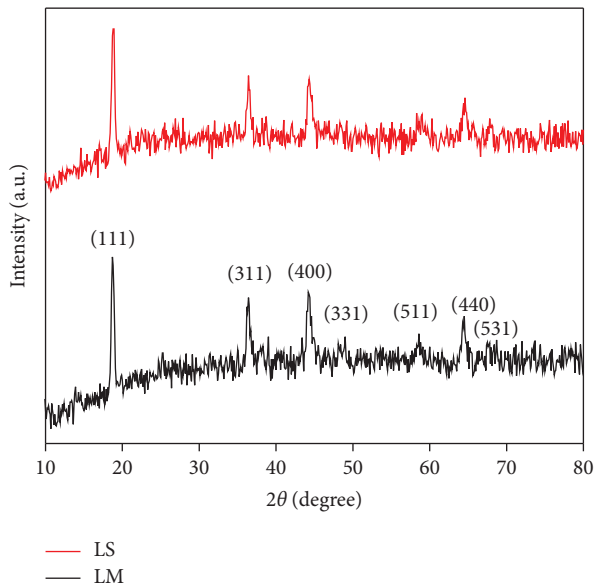
FIGURE 1: XRD pattern of (a) $Li_4Mn_5O_{12}$ and (b) $Li_4Mn_{4.75}Sm_{0.25}O_{12}$.

doping manganese with samarium. In addition, when no other peaks have been notified as impurities, the dopant enters into the lattice structure perfectly. On the other hand, the intensity of the peak decreases with doping. Using the Scherrer formula, the lattice constant and grain size of the prepared materials are calculated and presented in Table 1. It is also noticed that the crystallite size decreases with doping indicating that rare earth elements hinder the growth of pristine materials. Lattice density is calculated using the formula $\rho = 8M/Na^3$, where M, N, and a takes its usual meaning. Figures 2(a) and 2(b) represent the Williamson Hall plot of LM and LS. The broadening in the peak will cause defects in the crystal which also induces strain. The microstrain and crystallite size can also be calculated using the W H plot by considering $4 \sin \theta$ along the x-axis and $\beta \cos \theta$ along the y-axis as shown in Table 1. Using the linear fitting method, the slope and intercept are calculated for both the samples and the obtained crystallite size, which are closer to the values obtained from the Scherrer formula [24]. The formation of a positive slope indicates the presence of tensile strain in the compound [25, 26].

The nature of the chemical bond present in the compound can be studied with the help of FTIR. The fingerprint region (500–1500 cm^{-1}) exhibits the details about the type of metal-oxygen bond. The sharp peak observed from 555 to 640 cm^{-1} attributes to the symmetric stretching vibrations of the MO_6 octahedral group [20]. The characteristic peak around 1000 cm^{-1} corresponds to stretching vibrations of metal = oxygen bond for both the materials. A trace of C–O vibrational mode is noticed near at 1520 cm^{-1} which may be due to the carbon content present in the atmosphere or may be due to calcinations of the material in the muffle furnace [20]. Due to the adsorption of water molecules, a peak is noticed near 1640 cm^{-1}. A weak peak is observed at 2975 cm^{-1} which may be due to COO^- present on the surface of the material (Figure 3).

SEM and TEM analysis are powerful tools to study about the morphological features such as the shape and size of the prepared samples. Figure 4 explicits the SEM images of pure and Sm-doped $Li_4Mn_5O_{12}$. Both samples show the formation of polyhedral-shaped particles with slight agglomeration [27, 28]. The size of the particle is reduced when doped with samarium which may be due to the dopant inhibitng the growth of the particles which is an important factor to obtain a better electrical performance from the material [29]. Compared to pure $Li_4Mn_5O_{12}$, samarium-doped $Li_4Mn_5O_{12}$ exhibits more agglomeration. Since the boundaries are not clear, it is not possible to measure the length of the particles. The elemental analysis of the prepared materials is studied from the perspective of energy dispersive spectrum. Figures 4(e) and 4(f) show the EDX spectrum of both the samples, which also has clearly proven the presence of Mn, O, and Sm in appropriate concentrations in the spinel material. In addition, EDS mapping is recorded for both the compounds and it shows the homogenous distribution/presence of Mn and O in LM; Mn, O, and Sm in LS explains clearly the presence of dopant in the prepared material (Figure 5).

To reveal the morphology of the particles in more detail, TEM and HRTEM analysis are carried out for pure and samarium-doped lithium manganese oxide and its selected area diffraction pattern (SAED) is shown in Figure 6. The formation of polyhedral-shaped particles is more clearly confirmed from the TEM analysis and is also shown in Figures 6(a) and 6(d). The interplanar distances are calculated as 0.48 nm for both pure and Sm-doped material obtained from the lattice fringes which correspond to the high intensity (111) plane, respectively. From the SAED pattern (Figures 6(c) and 6(e)), the formation of bright spots with ring-like structures authenticates the polycrystalline nature of the prepared material [30]. For LM, the bright spot corresponds to the (111), (311), (400), (331), (511), and (440) planes; whereas for LS, it corresponds to (111), (311), (400), (331), and (511) planes which are in good agreement with the XRD data. The standard d-spacing values, obtained results, and calculated values from the SAED pattern are given in Table 2.

The complex impedance spectroscopy will give clear information about the electrical behavior of the material over a wide frequency. For the prepared $Li_4Mn_5O_{12}$ and $Li_4Mn_{4.9}Sm_{0.1}O_{12}$, the Nyquist plots are shown in Figures 7(a) and 7(b). Both the samples exhibit the formation of a single semicircle at a high-frequency region and the spike corresponds to the low-frequency region. By increasing the temperature, the diameter of the circle reduces. Normally, R_{ct}-charge-transfer resistance is obtained from the diameter of the semicircle due to the electrode-electrolyte interface, whereas the solid-state diffusion process exists from the appearance of a straight line at the low-frequency region implicit the Warburg diffusion [28, 31]. The calculated R_{ct} is tabulated and given in Table 3 for both the samples. On comparing both the samples, LS exhibited the lowest R_{ct} at all temperatures and the lowest value is obtained at 100°C, indicating that the sample may exhibit fast Li insertion/ deinsertion process than LM and may also account for the good cycling stability. Since LS exhibits lower charge-

TABLE 1: XRD parameters of LM and LS.

Material	Lattice parameter (Å)	Crystallite size(nm)		Lattice density $\times 10^6$	Slope ($\times 10^{-4}$)	Microstrain
		Scherrer formula	W H plot			
LM	8.176	16.03	16.25	12.01	4.55	0.00853
LS	8.174	12.62	13.39	12.60	4.31	0.01035

(a)

(b)
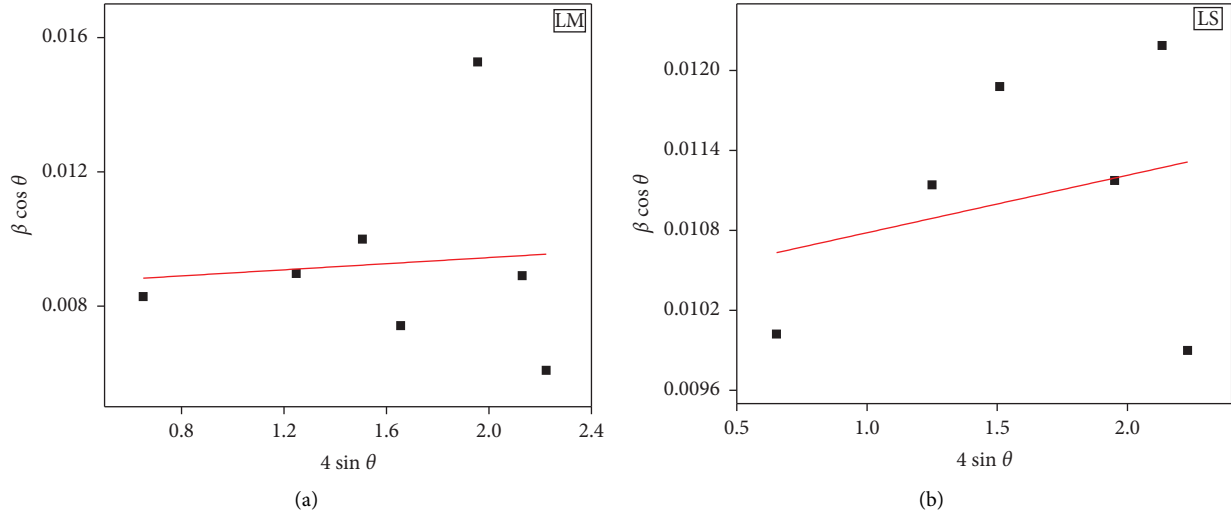
FIGURE 2: W-H plot of (a) $Li_4Mn_5O_{12}$ and (b) $Li_4Mn_{4.75}Sm_{0.25}O_{12}$.
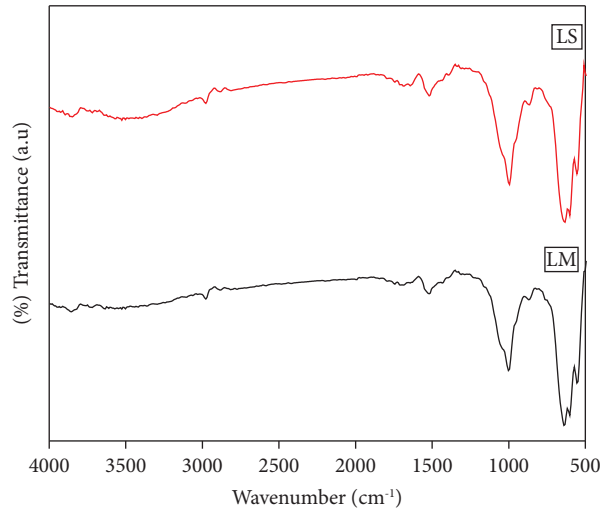
FIGURE 3: FT-IR spectrum of (a) $Li_4Mn_5O_{12}$ and (b) $Li_4Mn_{4.75}Sm_{0.25}O_{12}$.

transfer resistance, it may extend good electrical conductivity. It is also associated with the particle size that facilitates Li^+ transfer [32].

The frequency vs conductivity spectra are given in Figures 7(c) and 7(d) at different temperatures. Both the spectra exhibit a plateau at low frequency and dispersion at high frequency irrespective of temperatures. Due to the random mobility of ions, the dispersion can be observed at high-frequency regions. By extrapolating the plateau at the

y-axis, the dc conductivity of the samples can be determined, and the material was found to obey universal Jonscher's power law [20]. The conductivity obtained from the graph is given in Table 3, and the values are found to increase with the increase in temperature, which elucidates the thermally activated process [23]. Compared to pure LM, Sm-doped material (LS) exhibits very good electrical property indicating that optimum doping can influence the electrical behavior of the material.
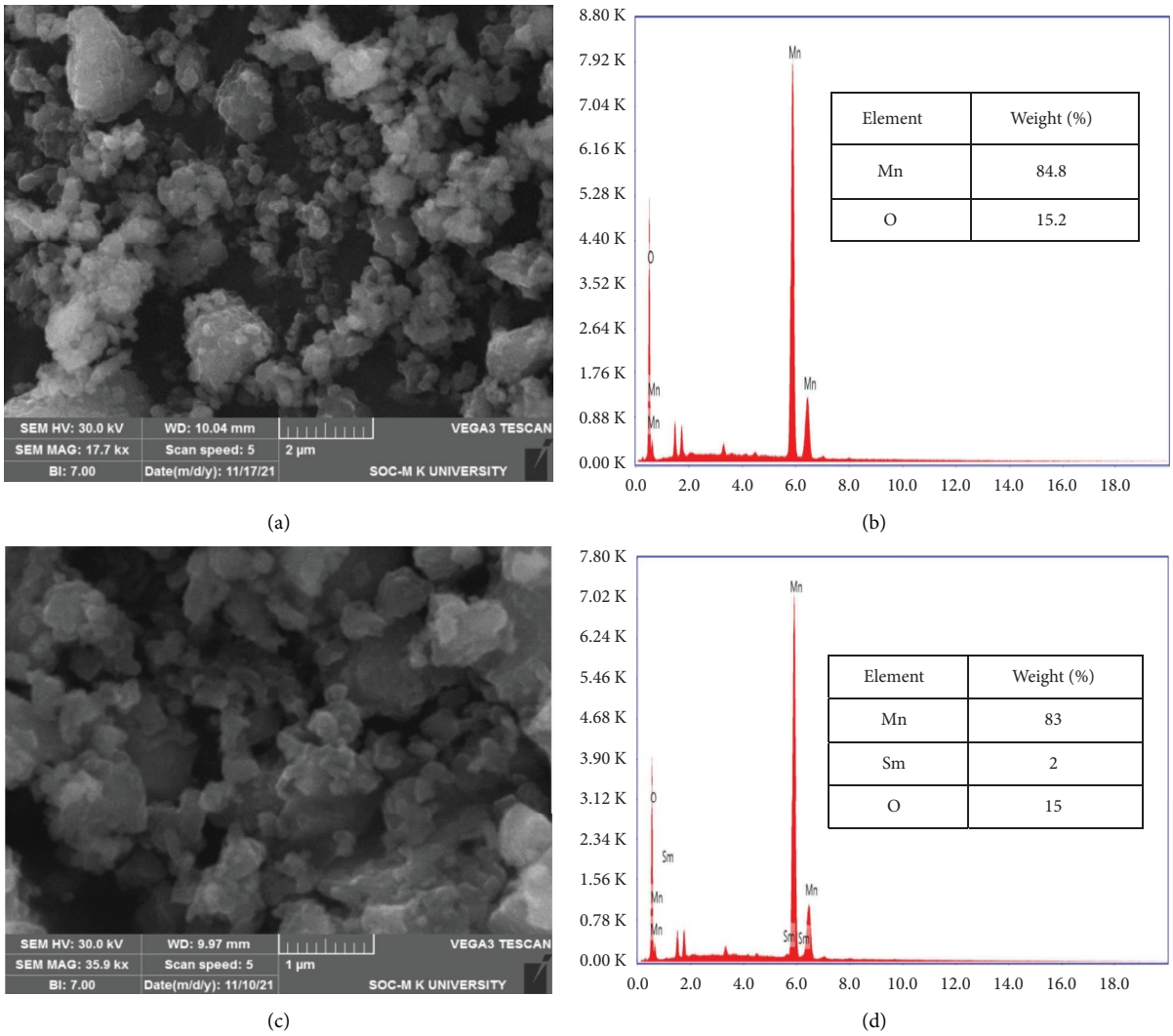
(a)

(b)

(c)

(d)

FIGURE 4: (a, c) SEM images and (b, d) EDX spectrum of $Li_4Mn_5O_{12}$ and $Li_4Mn_{4.75}Sm_{0.25}O_{12}$.

(a)

(b)
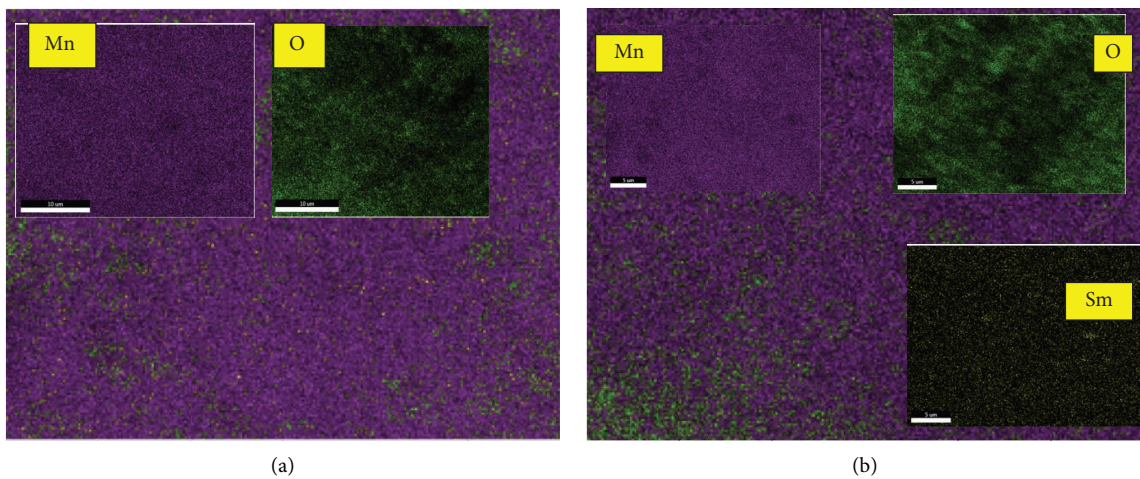
FIGURE 5: Elemental analysis of (a) $Li_4Mn_5O_{12}$ and (b) $Li_4Mn_{4.75}Sm_{0.25}O_{12}$ by EDS mapping.

(a)

(b)

(c)

(d)

(e)

(f)
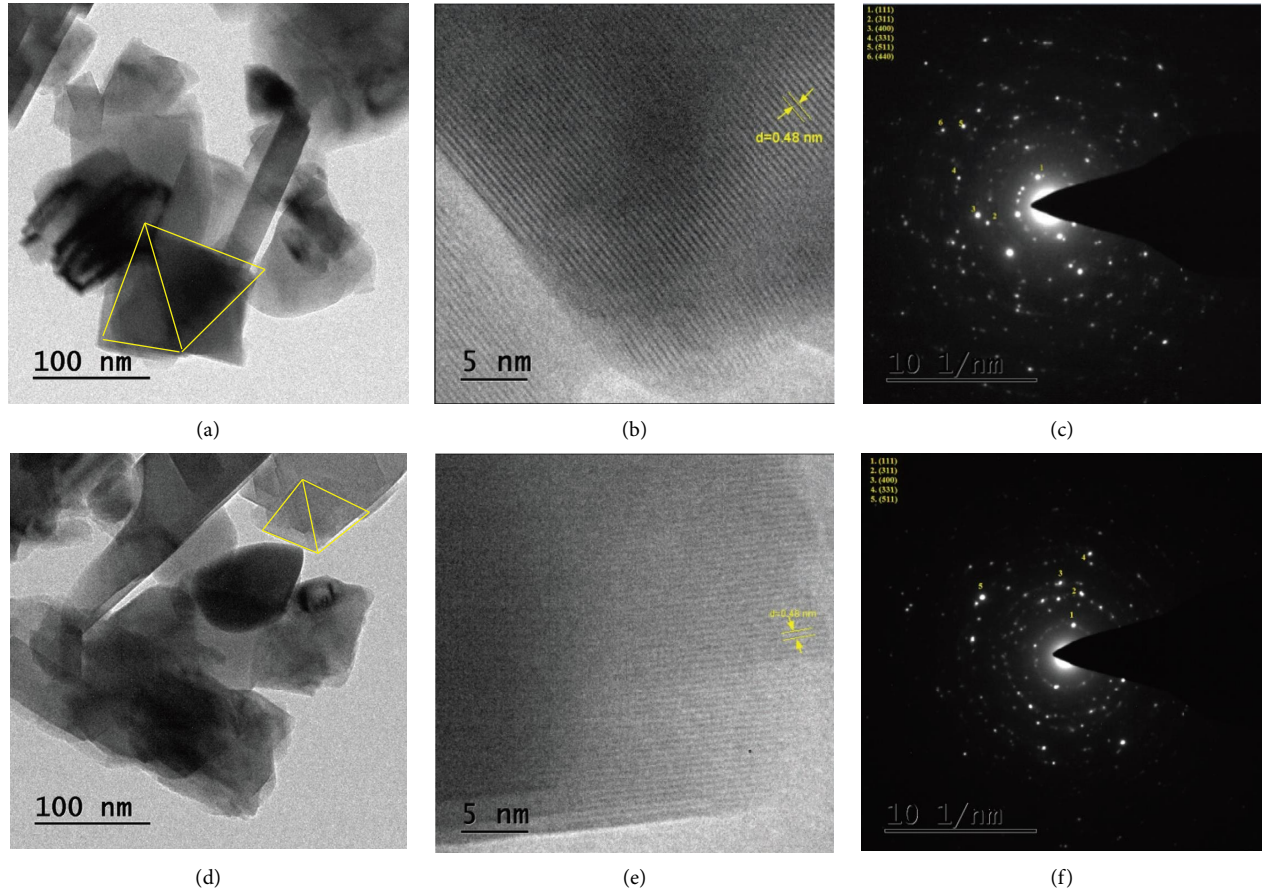
FIGURE 6: TEM and HRTEM images of (a, b) $Li_4Mn_5O_{12}$ and (d, e) $Li_4Mn_{4.75}Sm_{0.25}O_{12}$ and its corresponding SAED pattern (c, f).

TABLE 2: Comparison of d-spacing from the XRD and SAED pattern.

hkl plane	PowderX software	From XRD data		SAED pattern	
		LM	LS	LM	LS
(111)	4.71	4.73	4.72	4.70	4.75
(311)	2.46	2.46	2.46	2.41	2.50
(400)	2.04	2.04	2.04	2.12	2.06
(331)	1.87	1.86	—	1.69	1.64
(511)	1.57	1.57	1.57	1.41	1.47
(440)	1.44	1.44	1.44	1.27	—
(531)	1.37	1.38	1.38	—	—

The dielectric constant (ε') and tangent loss of the materials are examined at different temperatures and shown in Figures 8(a) and 8(b). From the figure, it is observed that, with the increase in frequency, the dielectric constant decreases and it increases with temperature and it becomes significant at low frequency. Due to space charges, the ε' decreases which leads to a high dielectric constant [32]. The inset Figures of 8(a) and 8(b) indicate the tangent loss vs frequency curve with respect to temperature. By increasing the temperature, the tangent loss (δ) decreases which indicates the dielectric relaxation of both the materials.
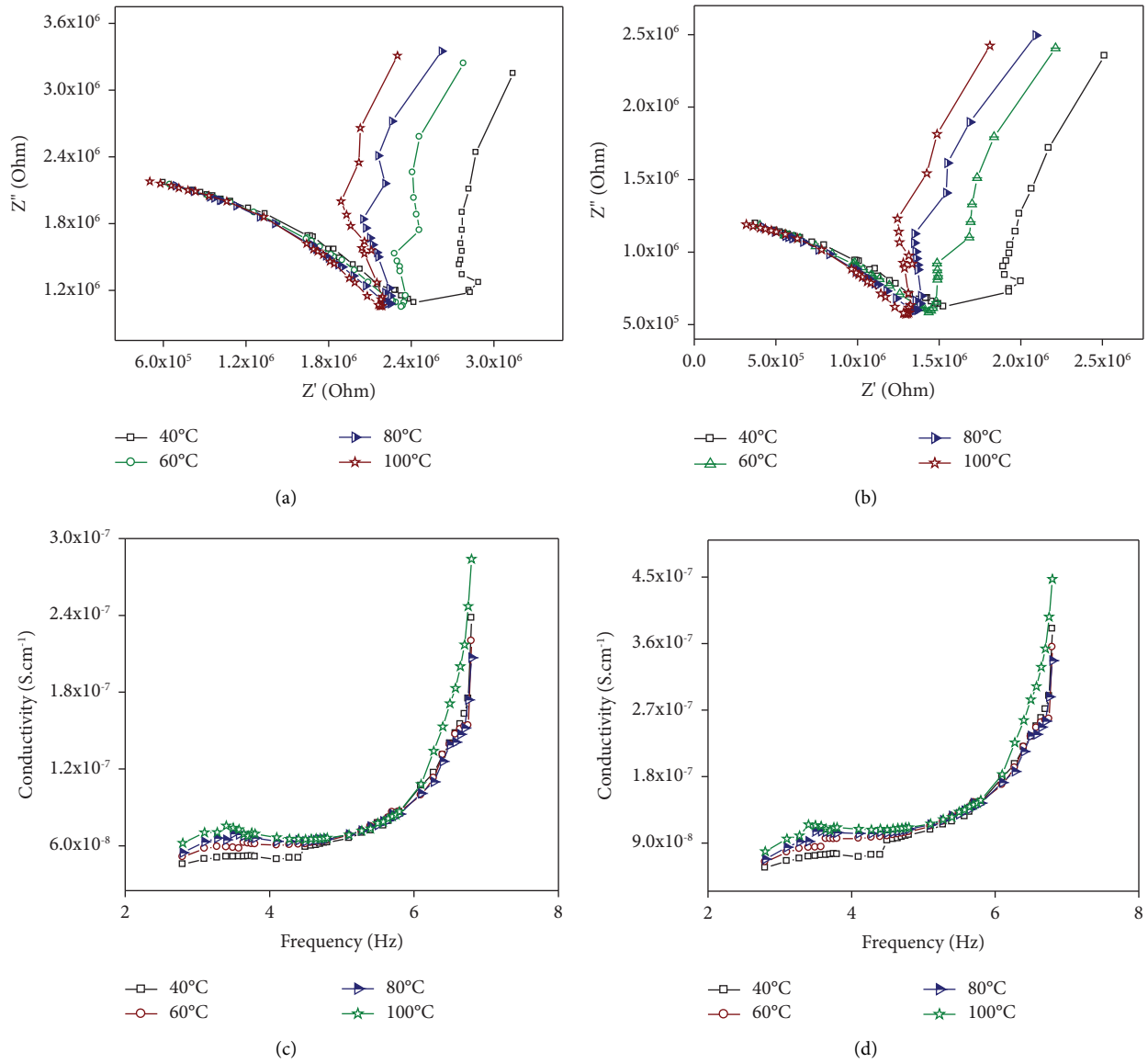
FIGURE 7: (a, b) Nyquist plots of LM and LS and (c, d) conductance spectra of LM and LS.

TABLE 3: Electrical parameters of LM and LS.

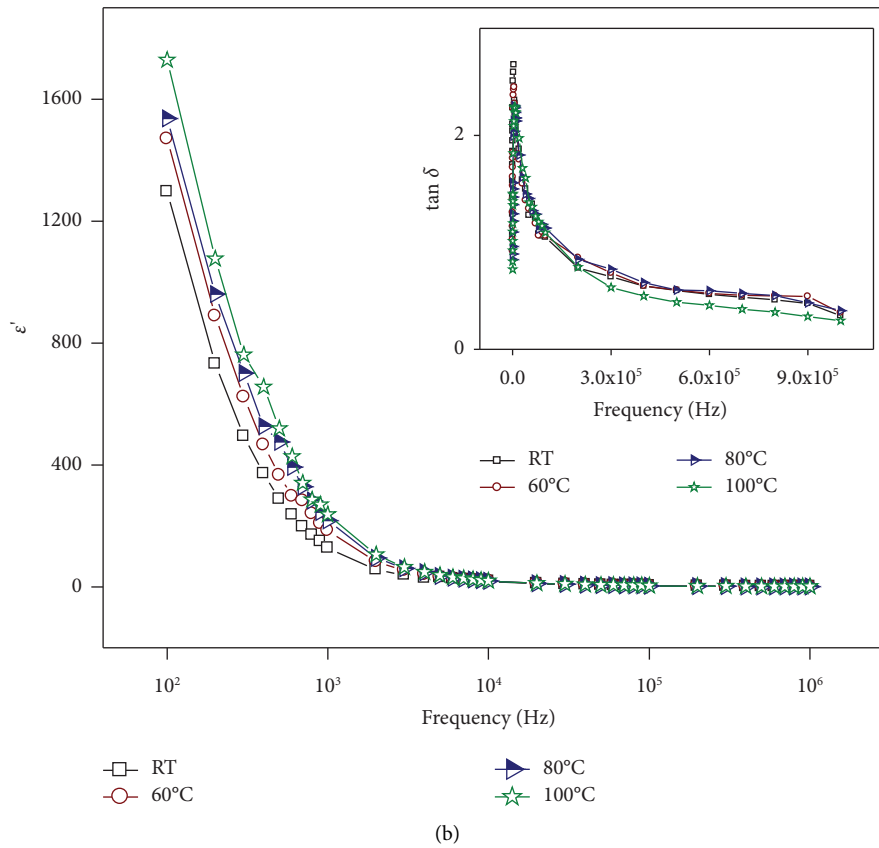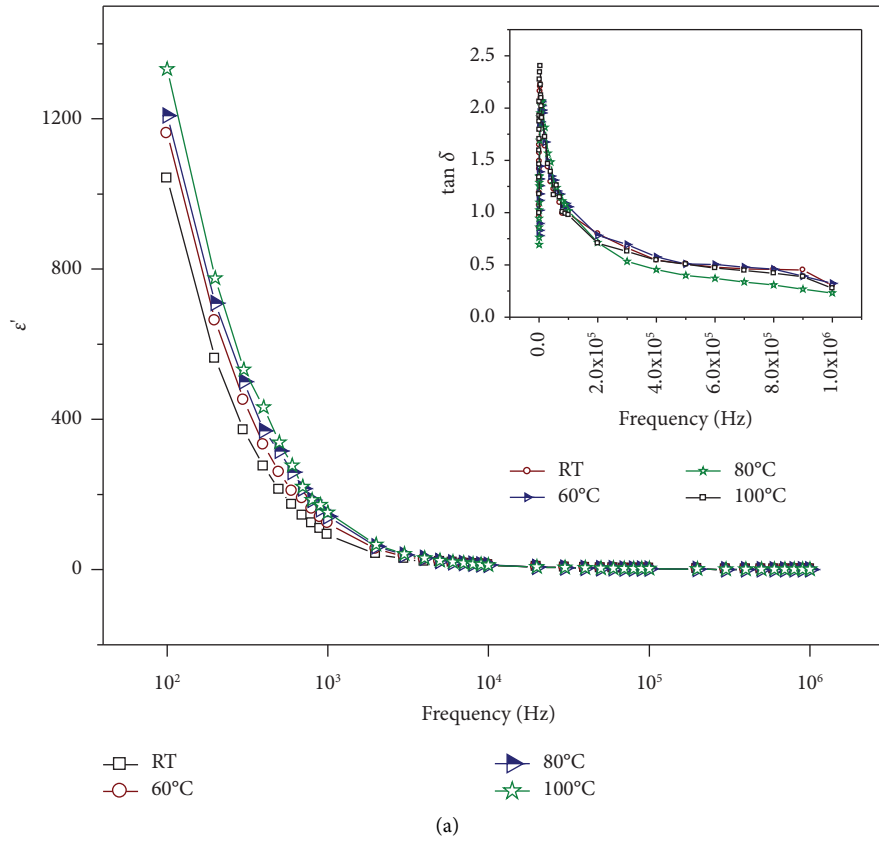| Temperature (°C)	$Li_4Mn_5O_{12}$		$Li_4Mn_{4.9}Sm_{0.1}O_{12}$	
	R_{ct} ($\times 10^6 \, \Omega$)	Conductivity ($\times 10^{-7}$ S.cm^{-1})	R_{ct} ($\times 10^6 \, \Omega$)	Conductivity ($\times 10^{-7}$ S.cm^{-1})
Room temperature	2.42	0.515	1.52	0.584
60	2.34	0.581	1.43	0.884
80	2.24	0.643	1.35	1.05
100	2.17	0.683	1.29	1.15

(a)

(b)

FIGURE 8: Dielectric constant as a function of frequency at different temperatures for LM (a) and LS (b) inset shows corresponding tangent loss.

4. Conclusion

Ball-milling assisted solid-state approach is used successfully to produce pure and doped lithium manganese oxides. The XRD pattern reveals a good crystalline nature and high material purity with a cubic spinel structure. Three crystallite sizes of the materials are calculated by the Scherrer formula and W H plot and it is found that compared to pure, Sm-doping exhibits smaller particle size. The stretching and vibration modes are notified from the prepared samples. The particles exhibit polyhedral morphology with slight agglomeration. The interplanar distance is calculated from the SAED pattern and matches with the XRD results. The substitution of Sm as a dopant at Mn sites has enhanced the conductivity of $Li_4Mn_5O_{12}$. The dopant can demonstrate good conducting qualities at $100^\circ C$ (1.15×10^{-7} $S\,cm^{-1}$), indicating that the dopant can enhance the electrical property and the material can operate as a good electrode for batteries, according to complex impedance spectroscopy.

Data Availability

The data generated or analyzed during this study are included within the article.

Conflicts of Interest

The authors declare that they have no conflicts of interest.

References

[1] J. M. Tarascon and M. Armand, "Issues and challenges facing rechargeable lithium batteries," *Nature*, vol. 414, no. 6861, pp. 359–367, 2001.

[2] Z. Zheng, P. Li, J. Huang et al., "High performance columnar-like Fe2O3@carbon composite anode via yolk@shell structural design," *Journal of Energy Chemistry*, vol. 41, pp. 126–134, 2020.

[3] L. J. Fu, H. Liu, C. Li et al., "Electrode materials for lithium secondary batteries prepared by sol–gel methods," *Progress in Materials Science*, vol. 50, no. 7, pp. 881–928, 2005.

[4] A. Sakuda, N. Nakamoto, H. Kitaura, A. Hayashi, K. Tadanaga, and M. Tatsumisago, "All-solid-state lithium secondary batteries with metal-sulfide-coated LiCoO2 prepared by thermal decomposition of dithiocarbamato complexes," *Journal of Materials Chemistry*, vol. 22, no. 30, pp. 15247–15254, 2012.

[5] J. Wang, J. Yang, Y. Tang et al., "Surface aging at olivine LiFePO4: a direct visual observation of iron dissolution and the protection role of nano-carbon coating," *Journal of Materials Chemistry*, vol. 1, no. 5, pp. 1579–1586, 2013.

[6] L. X. Yuan, Z. H. Wang, W. X. Zhang et al., "Development and challenges of LiFePO4cathode material for lithium-ion batteries," *Energy &amp; Environmental Science*, vol. 4, no. 2, pp. 269–284, 2011.

[7] Q. Shi, L. Xue, Z. Wei, F. Liu, X. Du, and D. D. DesMarteau, "Improvement in LiFePO4–Li battery performance via poly(perfluoroalkylsulfonyl)imide (PFSI) based ionene composite binder," *Journal of Materials Chemistry*, vol. 1, no. 47, pp. 15016–15021, 2013.

[8] A. M. Hashem, S. M. Abbas, X. U. Hou, A. L. Eid, and A. E. Abdel-Ghany, "Facile one step synthesis method of spinel LiMn2O4 cathode material for lithium batteries," *Heliyon*, vol. 5, no. 7, Article ID e02027, 2019.

[9] Y. Dai, L. Cai, and R. E. White, "Capacity fade model for spinel $LiMn_2O_4$ electrode," *Journal of the Electrochemical Society*, vol. 160, 2012.

[10] S. B. Schougaard, J. Breger, M. Jiang, C. P. Grey, and J. B. Goodenough, "LiNi0.5+δMn0.5−δO2—a high-rate, high-capacity cathode for lithium rechargeable batteries," *Advances in Materials*, vol. 18, no. 7, pp. 905–909, 2006.

[11] H. Yang, H.-H. Wu, M. Ge et al., "Simultaneously dual modification of Ni rich layered oxide cathode for high energy lithium ion batteries," *Advanced Functional Materials*, vol. 29, no. 13, Article ID 1808825, 2019.

[12] T. Rajkumar, K. Radhakrishnan, C. Rajaganapathy, S. P. Jani, and N. Ummal Salmaan, "Experimental investigation of AA6063 welded joints using FSW," *Advances in Materials Science & Engineering*, vol. 2022, Article ID 4174210, 10 pages, 2022.

[13] R. Yu, X. Zhang, T. Liu et al., "Spinel/layered heterostructured lithium-rich oxide nanowires as cathode material for high-energylithium-ion batteries," *ACS Applied Materials & Interfaces*, vol. 9, no. 47, pp. 41210–41223, 2017.

[14] X. Bian, Q. Fu, H. Qiu et al., "High-performance Li(Li0.18Ni0.15Co0.15Mn0.52)O2@Li4M5O12 heterostructured cathode material coated with a lithium borate oxide glass layer," *Chemistry of Materials*, vol. 27, no. 16, pp. 5745–5754, 2015.

[15] J. Zhang, R. Gao, L. Sun et al., "Understanding the effect of an in situ generated and integrated spinel phase on a layered Li-rich cathode material using a non-stoichiometric strategy," *PCCP: Physical Chemistry Chemical Physics*, vol. 18, no. 36, pp. 25711–25720, 2016.

[16] P. Ram, A. Gören, S. Ferdov et al., "Improved performance of rare earth doped LiMn2O4 cathodes for Lithium-ion battery applications," *New Journal Chemistry*, vol. 40, pp. 6244–6252, 2016.

[17] H. Sun, Y. Chen, C. Xu, D. Zhu, and L. Huang, "Electrochemical performance of rare-earth doped LiMn2O4 spinel cathode materials for Li-ion rechargeable battery," *Journal of Solid State Electrochemistry*, vol. 16, no. 3, pp. 1247–1254, 2012.

[18] S. Balaji, T. M. Chandran, and D. Mutharasu, "A study on the influence of dysprosium cation substitution on the structural, morphological, and electrochemical properties of lithium manganese oxide," *Ionics*, vol. 18, no. 6, pp. 549–558, 2012.

[19] S. Sharmila, B. Janarthanan, and J. Chandrasekaran, "Structural and electrical properties of Li_4 $Mn_{4.9}Ni_{0.1}O_{12}$ as a cathode material for rechargeable Li-ion batterie," *IOSR Journal of Applied Physics*, vol. 8, p. 52, 2016.

[20] S. Sharmila, B. Janarthanan, and J. Chandrasekaran, "Synthesis and characterization of Co-doped lithium manganese oxide as a cathode material for rechargeable Li-ion battery," *Ionics*, vol. 22, no. 9, pp. 1567–1574, 2016.

[21] S. Sharmila, B. Janarthanan, and J. Chandrasekaran, "Preparation and characterization of pure and Ti4+doped Li4Mn5O12 spinels as cathodes for Li-ion batteries," *International Journal of Scientific Engineering and Research*, vol. 6, p. 1763, 2015.

[22] K. K. Shaji, S. Sharmila, G. Sushama, B. Janarthanan, and J. Chandrasekaran, "Effect of molybdenum on Li2Mn4O9 for rechargeable lithium ion batteries," *Ionics*, vol. 24, no. 12, pp. 3725–3731, 2018.

[23] S. M. Vedhanayagam, S. Saminathan, B. Janarthanan, and J. Chandrasekaran, "Impedance analysis of zirconium-doped

lithium manganese oxide," *Bulletin of Materials Science*, vol. 43, no. 1, p. 294, 2020.

[24] C. Murugesan and G. Chandrasekaran, "Impact of Gd^{3+} substitution on the structural, magnetic and electrical properties of cobalt ferrite nanoparticles," *RSC Advances*, vol. 5, no. 90, pp. 73714–73725, 2015.

[25] A. Ahlawat, V. G. Sathe, V. R. Reddy, and A. Gupta, "Mossbauer, Raman and X-ray diffraction studies of superparamagnetic NiFe2O4 nanoparticles prepared by sol–gel auto-combustion method," *Journal of Magnetism and Magnetic Materials*, vol. 323, no. 15, pp. 2049–2054, 2011.

[26] P. Archana, B. Janarthanan, S. Bhuvana, P. Rajiv, and S. Sharmila, "Concert of zinc oxide nanoparticles synthesized using Cucumis melo by green synthesis and the antibacterial activity on pathogenic bacteria," *Inorganic Chemistry Communications*, vol. 137, Article ID 109255, 2022.

[27] S. Sharmila, B. Senthilkumar, V. D. Nithya, K. Vediappan, C. W. Lee, and R. K. Selvan, "Electrical and electrochemical properties of molten salt-synthesized Li4Ti5−xSnxO12 (x=0.0, 0.05 and 0.1) as anodes for Li-ion batteries," *Journal of Physics and Chemistry of Solids*, vol. 74, no. 11, pp. 1515–1521, 2013.

[28] V. D. Nithya, R. Kalai Selvan, K. Vediappan, S. Sharmila, and C. W. Lee, "Molten salt synthesis and characterization of Li4Ti5−Mn O12 (x= 0.0, 0.05 and 0.1) as anodes for Li-ion batteries," *Applied Surface Science*, vol. 261, pp. 515–519, 2012.

[29] R. K. Selvan, C. O. Augustin, V. Sepelak, L. J. Berchmans, C. Sanjeeviraja, and A. Gedanken, "Synthesis and characterization of CuFe2O4/CeO2 nanocomposites," *Materials Chemistry and Physics*, vol. 112, no. 2, pp. 373–380, 2008.

[30] P. E. Saranya and S. Selladurai, "Facile synthesis of NiSnO3/ graphene nanocomposite for high-performance electrode towards asymmetric supercapacitor device," *Journal of Materials Science*, vol. 53, no. 23, pp. 16022–16046, 2018.

[31] K. Ding, J. Zhao, J. Zhou et al., "Preparation and Characterization of Dy-doped Lithium Titanate ($Li_4Ti_5O_{12}$)," *International Journal of Electrochemical Science*, vol. 11, p. 446, 2016.

[32] P. Ram, A. Gören, S. Ferdov et al., "Synthesis and improved electrochemical performance of LiMn2−xGdxO4 based cathodes," *Solid State Ionics*, vol. 300, pp. 18–25, 2017.